Intervertebral Disc Mechanics With Nucleotomy: Differences Between Simple and Dual Loading

Bo Yang
Department of Mechanical Engineering,
University of California Berkeley,
Etcheverry Hall,
Berkeley, CA 94720

Eric Klineberg
Department of Orthopaedic Surgery,
University of California, Davis,
Davis Medical Center,
Sacramento, CA 95817

Grace D. O'Connell[1]
Department of Mechanical Engineering,
University of California Berkeley,
5122 Etcheverry Hall, #1740,
Berkeley, CA 94720;
Department of Orthopaedic Surgery,
University of California, San Francisco,
San Francisco, CA 94142
e-mail: g.oconnell@berkeley.edu

Painful herniated discs are treated surgically by removing extruded nucleus pulposus (NP) material (nucleotomy). NP removal through enzymatic digestion is also commonly performed to initiate degenerative changes to study potential biological repair strategies. Experimental and computational studies have shown a decrease in disc stiffness with nucleotomy under single loading modalities, such as compression-only or bending-only loading. However, studies that apply more physiologically relevant loading conditions, such as compression in combination with bending or torsion, have shown contradicting results. We used a previously validated bone–disc–bone finite element model (Control) to create a Nucleotomy model to evaluate the effect of dual loading conditions (compression with torsion or bending) on intradiscal deformations. While disc joint stiffness decreased with nucleotomy under single loading conditions, as commonly reported in the literature, dual loading resulted in an increase in bending stiffness. More specifically, dual loading resulted in a 40% increase in bending stiffness under flexion and extension and a 25% increase in stiffness under lateral bending. The increase in bending stiffness was due to an increase and shift in compressive stress, where peak stresses migrated from the NP–annulus interface to the outer annulus. In contrast, the decrease in torsional stiffness was due to greater fiber reorientation during compression. In general, large radial strains were observed with nucleotomy, suggesting an increased risk for delamination or degenerative remodeling. In conclusion, the effect of nucleotomy on disc mechanics depends on the type and complexity of applied loads. [DOI: 10.1115/1.4050538]

Keywords: nucleus pulposus, intervertebral disc, nucleotomy, finite element method, degeneration

1 Introduction

Partial removal of the nucleus pulposus (NP) is performed clinically to treat painful herniated discs [1]. Experimental and computational studies showed that NP removal affects disc joint mechanics and intradiscal deformations [2–6]. Nucleotomy decreases disc joint stiffness in torsion, bending, and shear, resulting in an increase in range of motion and contact forces at the facet joints [2,3]. Internally, nucleotomy decreases intradiscal pressure under compression, resulting in inward bulging of the inner AF and greater maximum AF strains [4–9]. However, most of these studies evaluated disc joint mechanics under single loading modalities, such as compression- or bending-only loading, which is not representative of complex in vivo loading conditions.

Few studies have evaluated disc mechanics under complex loading conditions. Previous work showed that disc joint torsional and shear stiffness is dependent on the compressive preload [10–14]. Recent studies applied complex six degrees-of-freedom loading and successfully initiated the disc failure in intact discs [15,16]. These findings have been valuable for directing computational models to apply complex load conditions on discs [17]; however, quantifying the role of each loading modality to failure has been difficult due to the wide range of loading configurations applied simultaneously.

Moreover, there has been limited research investigating the effect of nucleotomy on disc mechanics and several reports provide contradicting results. Both experimental and computational studies showed nucleotomy decreased disc shear stiffness and increased loading on the facet joint and ligaments [13,18]. Experiments from Frei and coworkers showed that nucleotomy increased extension stiffness, but did not affect flexion or lateral bending stiffness [19]. Similar to Frei et al., computational work from Shirazi-Adl and coworkers found that removing NP fluid increased extension stiffness, but there was a marked decreased in flexion and rotation stiffness [20]. Lastly, changes in lateral bending stiffness were found to be dependent on the amount of NP fluid removed [20].

Therefore, the aim of this study was to evaluate the effect of nucleotomy on disc mechanics using a finite element model of a bone-disc-bone that mimicked the anatomy of human cadaver specimens prepared for experimental testing. The effect of single versus dual loading on disc mechanics was evaluated. Dual loading was defined as a subset of complex loading, where axial compression was applied prior to bending (flexion, extension, and lateral bending) or rotation. We hypothesized that disc stiffness increases with nucleotomy when tested under dual loading conditions, but will decrease under single loading conditions. To test this hypothesis, we modified our previously validated finite element model of the human lumbar disc by removing the NP to create a total nucleotomy model [21]. Stiffness, internal stress, and strain distributions were evaluated for multiple loading conditions.

2 Method

2.1 Model Development. The Control model was a single bone–disc–bone with geometry based on 13 L3L4 human male

[1]Corresponding author.
Manuscript received January 12, 2020; final manuscript received February 19, 2021; published online April 21, 2021. Assoc. Editor: Christian Puttlitz.

discs averaged together (age range: 50–93 years, average age = 67.5 years, Pfirrmann degenerative grade range: 2.3–5.0, average degeneration = 3.3; disc height = 11 mm, disc area = 1949 mm^2, NP area = 546 mm^2, Fig. 1) [21,22]. The Control model included separate material descriptions for the NP and AF, which were sandwiched between cartilage and bony endplates with thicknesses of 0.8 and 0.6 mm, respectively (Fig. 1) [23,24]. The cartilage endplate (CEP) covered the entire NP and inner AF. Disc subcomponents and bones were welded together by sharing nodes at the interface. The AF was divided into 20 concentric layers [25] and each layer was subdivided into four anatomical regions to assign region-dependent material properties [26,27].

The NP, CEP, and AF matrix were modeled as isotropic hyperelastic Mooney–Rivlin materials. The AF was modeled as having nonlinear tension-only elastic fibers embedded within an extrafibrillar matrix. Material coefficients for NP, endplates, and AF matrix were selected from the literature (Table 1) [28], while fiber coefficients were calibrated using data from single lamellae tensile tests (Table 2) [26,29]. Therefore, the outer AF was stiffer than the inner AF and the anterior AF was stiffer than the posterior AF [26,27]. A cross-ply fiber architecture was defined, such that each adjacent lamellae had opposing fiber orientations. Fiber orientation decreased from ±43 deg in the innermost layer to ±28 deg in the outermost layer [30]. The cortical bone was described as a Neo–Hookean material (modulus = 12,000 MPa, Poisson's ratio = 0.3) [28]. The NP was completely removed from the Control model to create the Nucleotomy model, representing an extreme case of the nucleotomy procedure.

2.2 Model Simulation and Data Analyses. Our previous study validated disc joint mechanics of the Control model by comparing model results from single loading modalities (axial compression, torsion, flexion, extension, and lateral bending) to experimental data [21]. In short, the normalized change in disc height under axial compression and joint stiffness in bending agreed well with the literature [5,10,31]. Moreover, angular displacement–torque response in flexion, extension, lateral bending, and axial rotation agreed well with the behavior reported in the literature [2,32,33].

Two rigid bodies were defined to apply boundary and load conditions. One was attached to the upper surface of the superior vertebral body and the other was attached to the lower surface of the inferior vertebral body. The inferior rigid body was fixed in all degrees-of-freedom, while load and displacement were applied to the superior rigid body, which was free to rotate. A sliding contact was defined between the NP-AF and CEP-NP interfaces. A 936 N (0.48 MPa) compressive load was applied and angular displacements (4 deg in torsion, 6.5 deg in flexion, 4 deg in extension, or 5 deg in lateral bending, based on data for human lumbar discs) was applied with free axes of rotation (2 models X 4 simulations = 8 total simulations) [34–36]. During bending or rotation, angular displacements about the other axes were restricted to mimic loading conditions used for in vitro experiments [2,5]. Reaction torques due to these restrictions were measured. All simulations were conducted in FEBIO [37].

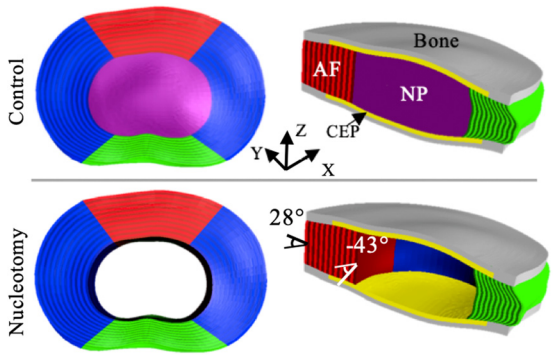

Fig. 1 Schematic of Control and Nucleotomy models. The annulus fibrosus (AF) was separated into four anatomical regions (red = anterior, blue = lateral, and green = posterior). Fiber orientation alternated between layers, decreasing from ±43 deg with respect to the horizontal plane in the inner AF to ±28 deg in the outer AF. The model also included material descriptions for the nucleus pulposus (NP, purple, only in Control model), cartilaginous endplates (CEP, yellow), and boney endplates (gray). (Color version online.)

The normalized change in disc height was calculated as displacement in the axial direction divided by the initial disc height. Compressive stress was averaged across all elements in the disc and plotted against the normalized change in disc height. Radial bulging was measured in the anterior, lateral, and posterior AF at the mid-disc height. Peak stress, strain, and stretch were calculated by sorting data for all elements and averaging the top 10%. Normalized compressive stiffness (MPa) was calculated as the slope of the stress–normalized displacement curve in the toe and linear regions. Torsional and bending stiffness (Nm/deg) was calculated as the slope of the torque–angular displacement curves. Stress and strain distributions were evaluated in the disc's anatomic directions (i.e., axial, radial, and circumferential directions). Fiber stretch and reorientation were calculated for each element, using the volume of each element as a weighting factor. A weighted average was calculated for each AF layer, which included data from the anterior, posterior, and lateral AF. The volume ratio of stretched fibers was defined the sum of element-volumes with loaded fibers divided by the total element-volume for the layer.

3 Result

3.1 Disc Joint Mechanics: Compression-Only Loading. The normalized change in disc height for the Nucleotomy model in axial compression was twofold greater than the Control model (2.63 mm or 23.9% versus 1.23 mm or 11.2%, Fig. 2(*a*)). Nucleotomy resulted in a 60% decrease in toe-region stiffness and a 40% decrease in linear-region stiffness (Fig. 2(*b*)). While a wide range of values have been reported in the literature for disc joint compressive modulus (intact = 4–25 MPa, partial or complete nucleotomy = 2–29 MPa) [1], our simulation results showed comparable relative trends (based on averaged data in the literature) [2]. Thus,

Table 1 Material parameters for the nucleus pulposus (NP), extrafibrillar matrix of the annulus fibrosus (AF), and cartilaginous endplate (CEP), which were described Mooney–Rivlin materials (c_1, c_2, k)

Property	NP	AF Matrix	CEP
c_1 (MPa)	0.05	0.09	0.55
c_2 (MPa)	0.01	0.01	0.01
k (MPa)	50	3	20

Table 2 Material coefficients for fibers in different regions of the annulus fibrosus

Region	AO	AI	PO	PI	LO	LI
E (MPa)	57	18	35	15	46	16.5
β	4	5	5	6	4.5	5.5
λ_0	1.01	1.07	1.03	1.10	1.02	1.09

AO: anterior-outer, AI: anterior-inner, LO: lateral-outer, LI: lateral-inner, PO: posterior-outer, and PI: posterior-inner. Fibers were described using a nonlinear strain energy density function, where E represents the linear region Young's modulus, β represents toe-region nonlinearity, and λ_0 represents the transition stretch between the toe and linear region.

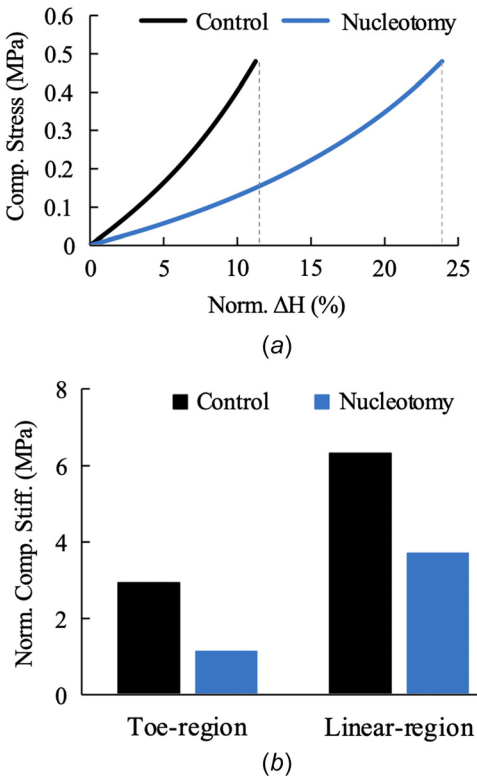

Fig. 2 (*a*) Compressive stress versus normalized change in disc height and (*b*) normalized compressive stiffness in the toe and linear regions, which was calculated as the slope of compressive stress versus normalized change in disc height. (Color version online.)

we considered the Nucleotomy model valid for assessing changes in intradiscal stress and strain distributions.

The outer surface of the AF and the NP-AF interface all bulged outward in the Control model with the outer surface bulging outwards more than the NP-AF interface (2.1 mm versus 1.5 mm in the anterior region, 1.8 mm versus 1.0 mm in the posterior region, and 1.6 mm versus 1.2 mm in the lateral region; Fig. 3). The outer surface of the AF in the Nucleotomy model bulged outward 10%–40% more than the Control model; however, the NP-AF interface bulged inward (Fig. 3). In the Control model, compression generated reaction torques of 2.20 N·m around the *X*-axis (flexion), 0.20 N·m around the *Y*-axis (lateral bending), and 0.09 N·m around the *Z*-axis (torsion). The response was comparable for the Nucleotomy model, with reaction torques of 2.22, 0.28, and 0.14 N·m around *X*-axis, *Y*-axis, and *Z*-axis, respectively.

3.2 Disc Joint Mechanics: Dual Loading Conditions. While torque versus angle of rotation for bending-only loading (i.e., no compressive preload) was nonlinear, a compressive preload resulted in linear torque-rotation behavior (Fig. 4(*a*)). Torsional stiffness decreased by more than 30% with nucleotomy. However, bending stiffness in flexion and extension increased by more than 40% and lateral bending stiffness increased by 25% with nucleotomy (Fig. 4(*b*)). Bending caused a reaction torque that was less than 0.2 N·m. Since dual-loading conditions provide a better representation of complex loading conditions experienced by the disc [38], further data analysis was performed on dual loading simulations, with compression-only loading used for comparison.

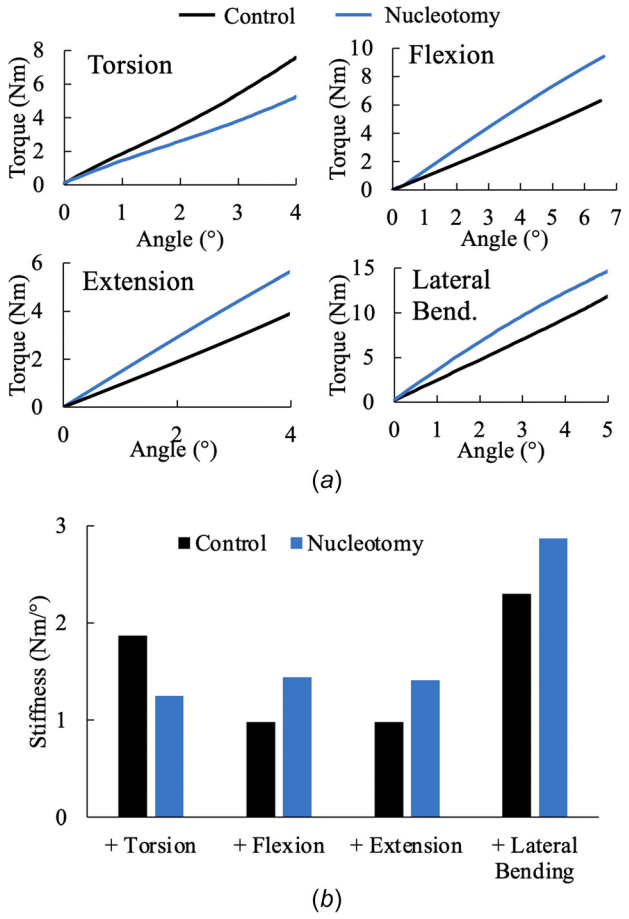

Fig. 4 (*a*) Torque versus rotation angle for Control (black) and Nucleotomy (blue) models under axial torsion, flexion, extension, and lateral bending and (*b*) disc joint stiffness was calculated as the slope of each torque–rotation curve. "+" for labels on the *x*-axis indicates that each loading condition was applied in combination with axial compression (948 N), which was applied prior to bending. (Color version online.)

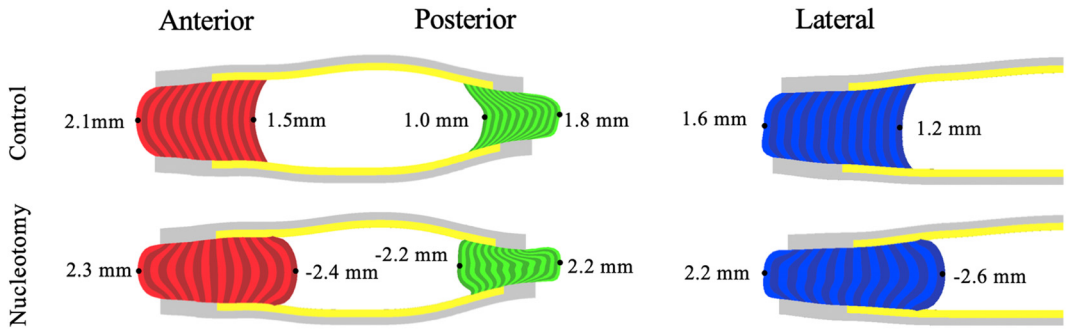

Fig. 3 Anterior, posterior, and lateral bulging at the outer AF and NP–AF interface, measured at the mid-disc height under 936 N of axial compression. Negative values represent inward bulging and positive values represent outward bulging with respect to the reference configuration. (Color version online.)

Bending increased outward bulging on the side of loading (e.g., anterior AF in flexion), but decreased the magnitude of outward bulging on the opposite side. For example, under extension, the Control model anterior AF bulging decreased by 60% (0.8 mm) and posterior AF bulging increased by ~30% (2.3 mm). Changes in outward radial bulging was more pronounced with Nucleotomy. Under extension, there was a 65% decrease in the anterior AF radial bulge and a 50% increase in the posterior AF radial displacement (2.1 mm). Axial rotation combined with compression resulted in minimal outward radial bulging for all annular regions in both models (bulge = 0.2–0.5 mm).

3.3 Stress Distributions. In the Control model, axial compressive stress at the midtransverse plane was greatest in the NP (NP: 0.63 MPa versus AF: <0.5 MPa; Fig. 5(*a*)). Peak axial compressive stresses in the AF shifted toward the outer posterolateral region with Nucleotomy, with a 57% increase in stress magnitude (Control = 0.51 MPa and Nucleotomy = 0.80 MPa; Fig. 5(*a*)—first column). Applying torsion after compression did not alter axial stress distributions in either the Control or Nucleotomy model (Fig. 5(*a*)—first column versus second column). Flexion, extension, and lateral bending combined with compression shifted the location of peak axial compressive stress toward the side of loading (Fig. 5(*a*)—third–fifth columns). In the Control model, peak axial compressive stresses were located in the inner or inner–middle AF. Removal of the NP slightly shifted the location of peak axial compressive stresses to the outer AF, resulting in a 50% increase in peak stress (0.89–1.36 MPa).

In the Control, the NP experienced high compressive stress in the radial and circumferential directions (magnitude > 0.5 MPa, Figs. 5(*b*) and 5(*c*)—first and third rows). The median radial-direction stress in the NP was –0.59 MPa (peak = –0.64 MPa). Similar to axial-direction compressive stress, bending resulted in a shift in the location of peak radial- and circumferential-direction stress and a slight increase in peak stress magnitude (5% increase). In the Nucleotomy model, peak compressive radial- and circumferential-direction stress occurred in the mid-AF and was located on the side of bending load (Figs. 5(*b*) and 5(*c*)—third–fifth columns). In both Control and Nucleotomy models, tensile circumferential direction stresses in the outer AF increased with bending and torsion (Fig. 5(*c*)—red regions) and greater tensile stresses occurring in the Control disc.

3.4 Strain Distributions. In the Control model, axial direction strains under compression were similar in the NP and AF, where peak compressive axial strains occurred at the mid-disc height (Fig. 6(*a*)—first column). NP removal resulted in a 65% increase in peak compressive axial strains in mid-disc height of the AF (–0.40 versus –0.24, Fig. 6(*a*)—first column). Applying torsion after compression did not alter axial strain maps (Fig. 6(*a*)—first column versus second column). Flexion, extension, and lateral bending in the Control model shifted the location

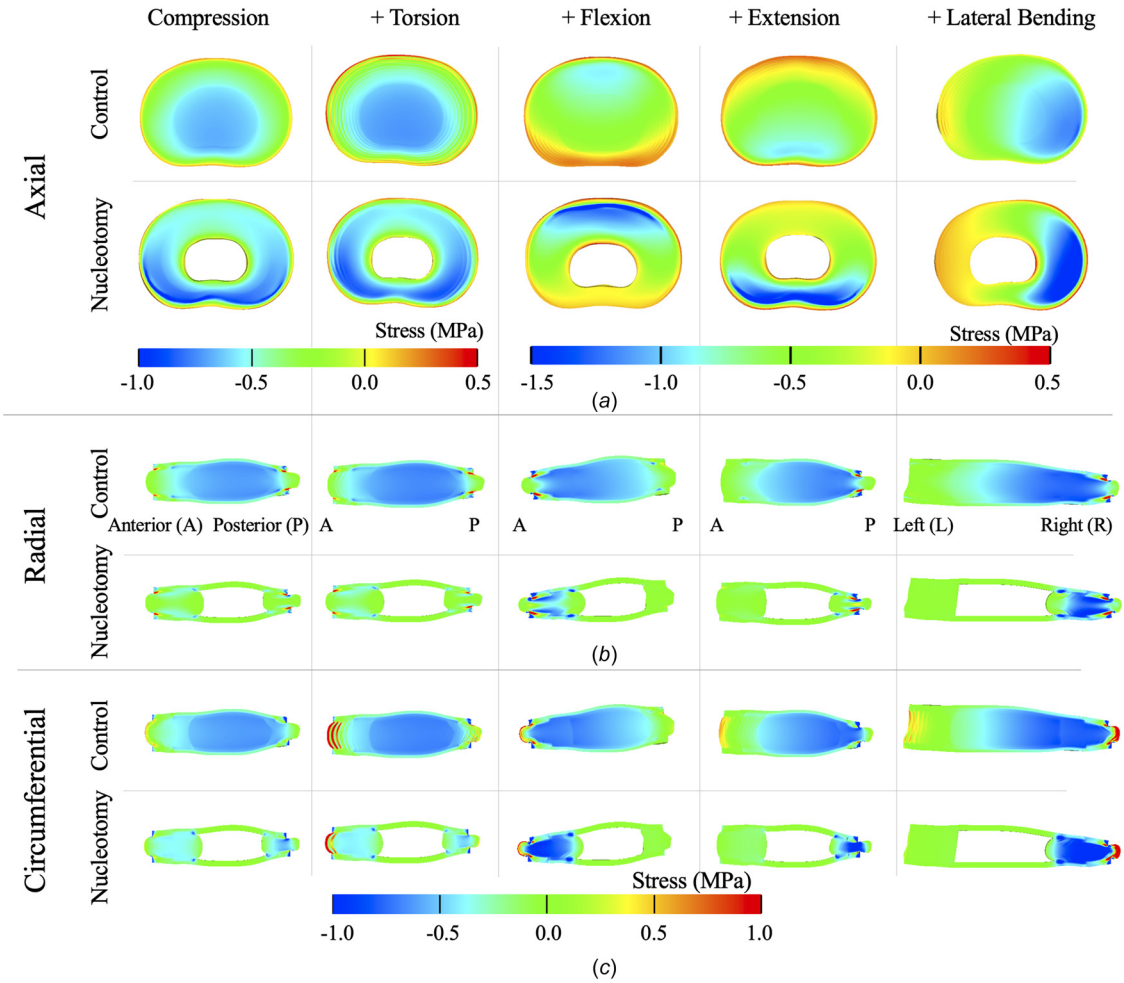

Fig. 5 (*a*) Axial stress distribution at the midtransverse plane and (*b*) radial and (*c*) circumferential direction stress distributions at the midsagittal plane for Control (top row) and Nucleotomy (bottom) models. Axial torsion, flexion, extension, or lateral bending was applied after axial compression (denoted by "+"). Peak compressive stress was ~50% greater in flexion, extension, and lateral bending; therefore, a separate legend was used for clarity. (Color version online.)

of peak compressive axial strains to the side of loading, whereas the opposite side experienced tensile axial strains (e.g., posterior AF under flexion; Fig. 6(*a*)—columns 3–5, top row). In contrast, in the Nucleotomy model, peak compressive axial strains occurred on the same side as peak tensile strains, with a 25% increase in strain magnitude when compared to the Control model (Fig. 6(*a*)—columns 3–5, bottom row).

Due to the poisson effect, large tensile radial strains developed at the location of peak compressive axial strains (Figs. 6(*a*) and 6(*b*)). Peak tensile radial strains in the Nucleotomy model were 2× greater than the Control model under pure compression (1.0 versus 0.3, Fig. 6(*b*)—first column). Similarly, large compressive radial strains developed at locations of tensile axial strains. Lastly, the magnitude of circumferential strains was much lower (<25%) than the magnitude of axial or radial strains (<0.1 versus <0.4; Fig. 6(*c*)). In the Control model, tensile circumferential direction strains were higher in the NP. With Nucleotomy, tensile circumferential direction strains only developed as localized strain concentrations at the innermost (i.e., extension) or outermost AF regions (e.g., flexion or lateral bending).

3.5 Fiber Stretch. In the Control model, 35% of inner AF fibers (i.e., stretch volume ratio ≈ 0.35) and ∼85% of outer AF fibers were loaded in tension during compression (Fig. 7(*a*)—black, Fig. 8(*a*)—first column). Nucleotomy decreased fiber engagement in the inner AF under compression, with only 20% of inner AF fibers loaded in tension. However, fiber engagement in the outer AF was not affected by Nucleotomy (Fig. 7(*a*)—blue). In the Control, fibers that were engaged during compression experienced relatively uniform stretch throughout the AF (average stretch ∼1.02; Fig. 7(*b*)). Layer-averaged fiber stretch in the inner AF increased 2–3-fold with nucleotomy (Fig. 7(*b*)—black versus blue "x"s).

Applying torsion after compression resulted in total fiber engagement in every other layer, where fibers were more aligned with the rotation direction, while fibers in adjacent layers were not loaded (Fig. 7(*c*)). Engagement of only half of the available fibers during torsion resulted in an increase in fiber stretch from 1.02 to over 1.04 (Figs. 7(*b*) versus 7(*d*)), where peak fiber stretch occurred in the posterior and posterior-lateral AF (Fig. 8(*a*)—second column). With Nucleotomy, fiber engagement under torsion followed a similar trend, but maximum fiber engagement in the inner AF was 40% lower than the Control (Fig. 7(*c*)), resulting in slight differences in fiber stretch (Figs. 7(*b*) versus 7(*d*)—blue lines). Nucleotomy did not alter fiber engagement and stretch in the outer AF during torsion with compression.

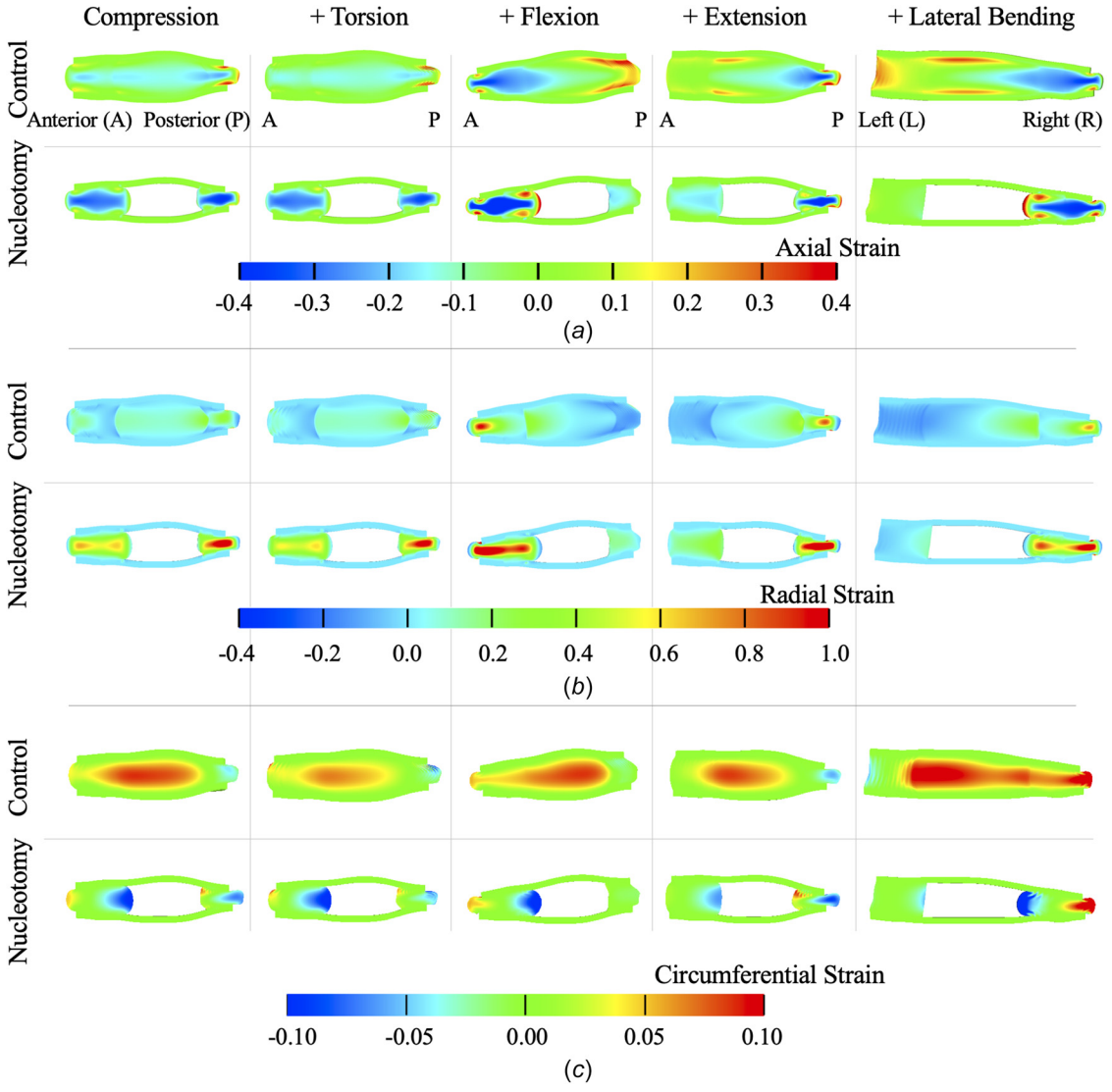

Fig. 6 (*a*) Axial, (*b*) radial, and (*c*) circumferential strain distributions at the midsagittal plane for Control (top row) and Nucleotomy (bottom row) models. "+" indicates axial torsion, flexion, extension, or lateral bending was applied after compression. (Color version online.)

Fiber engagement during bending with compression was relatively uniform throughout the AF, increasing in the outer 25% of the annulus (Fig. 7(*e*)). Bending increased inner AF fiber engagement by 50% in the Control. Similarly, in the Nucleotomy model, inner and mid-AF fiber engagement increased from relatively no fiber engagement to 20% of fibers being loaded (Figs. 7(*a*) versus 7(*e*)—blue lines) Although the Control model had a greater percentage of loaded fibers throughout the AF, the average fiber stretch of loaded fibers was less than 1.06 and was not affected by Nucleotomy (Figs. 7(*e*) and 7(*f*)). Fiber stretch in the Control was greatest in the anterior–lateral to lateral AF for all loading configurations with peak values less than 1.08 (Fig. 8(*a*)—third–fifth columns). However, the location of peak fiber stretch shifted to the side of bending with Nucleotomy (Fig. 8(*a*)—bottom row, columns 3–5). Thus, peak fiber stretch occurred in the posterior AF under extension and the anterior AF under flexion, and peak fiber stretch was slightly higher with Nucleotomy (<1.11).

3.6 Fiber Reorientation. Under axial compression, fibers reoriented toward the transverse plane; however, the magnitude of fiber reorientation was 2× greater with Nucleotomy (∼10 deg versus ∼5 deg; Fig. 9(*a*)). Furthermore, more fiber reorientation occurred in the posterior AF with Nucleotomy (Fig. 8(*b*)—first column). Torsion resulted in a zigzagged pattern in layer-averaged fiber reorientation, where AF layers with greater fiber stretch corresponded to layers with more fiber reorientation (Figs. 7(*d*) and 9(*b*)). Bending resulted in relatively few changes in fiber reorientation (Fig. 9(*a*)), but region-dependent changes were observed in both models (Fig. 8(*b*)—third–fifth columns). For example, flexion increased fiber reorientation in the anterior AF and decreased fiber reorientation in the posterior AF (Fig. 8(*b*)—first versus third column). Lastly, fibers in the inner AF of the Nucleotomy model reoriented away from the transverse plane, likely due to inward bulging of the AF (Fig. 8(*b*)).

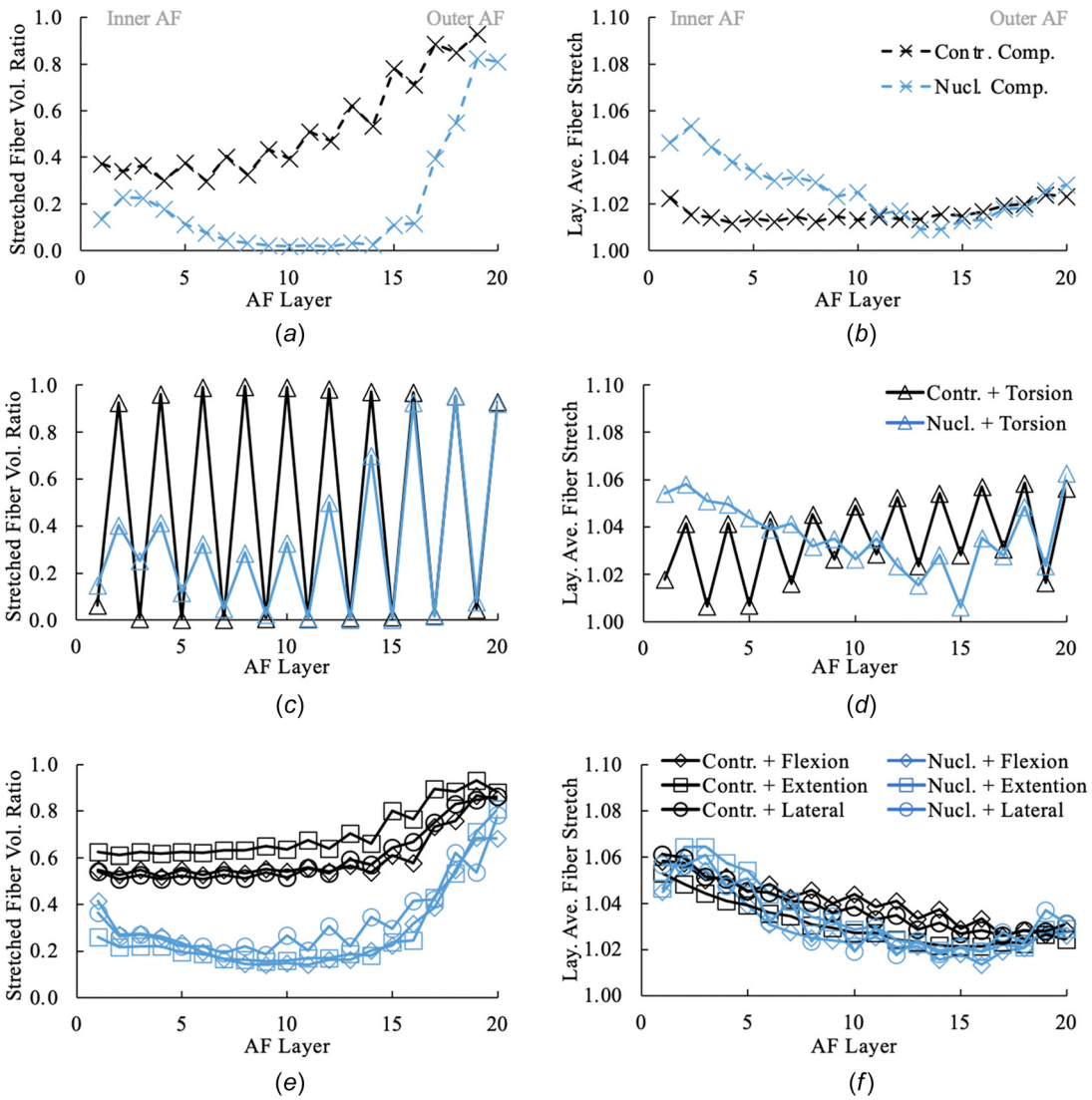

Fig. 7 Data shown in the left column represents volume ratio of fiber elements under tension for each lamellae, including data from the anterior, posterior, and lateral regions. Data shown in the right column represents layer-averaged fiber stretch with respect to lamellae layer. For all plots, Layer 1 represents the innermost layer and Layer 20 represents the outermost layer. Fiber stretch is shown for (*a,b*) compression-only loading, (*c,d*) compression with torsion, and (*e,f*) compression with bending. Black lines represent data the Control model and blue lines represent data from the Nucleotomy model. Figures in the same row shared the same legend. (Color version online.)

4 Discussion

Simulations showed that the effect of nucleotomy on disc joint mechanics depended on whether single or multiloading modalities were considered. Under compression- or bending-only loading, nucleotomy decreased stiffness, agreeing with previous experimental and computational studies [2–4,8,32,39]. However, dual loading, such as compression combined with bending, resulted in an increase in bending stiffness, suggesting that the disc is more resistant to bending after nucleotomy. The discrepancy between single- and dual-loading highlights the importance of evaluating disc joint mechanics under conditions that better represent the complex loading conditions experienced by the disc [15,17]. A recent review of the spine biomechanics literature highlighted the range and use of compressive preloading prior to bending, which leads to large differences in reported mechanical properties. Moving toward consensus in mechanical testing methodologies will make comparing results between studies easier [40]. However, this study shows how data from finite element models can complement experimental findings and allow for comparisons to be made between specimens and or different study designs [41].

The disc is often compared to a pressurized tire; however, the loss of NP pressure, either through severe degeneration or nucleotomy, causes the disc to behave more like a compressed O-ring with the AF absorbing much of the applied stress [42]. The Nucleotomy model demonstrated greater outward bulging of the outer AF, larger tensile radial strains, and inward bulging of the inner AF, agreeing well with experimental observations [4,5,8,9,43]. Large tensile radial strains occurred more frequently in the mid-AF and may lead to annular delamination, which is known to be more prevalent in older or degenerated discs [43–45]. Moreover, herniated discs have also been shown to have thicker lamellae, which may be a result of a tissue remodeling or permanent deformations from larger radial tensile strains [43,46,47].

The increase in joint stiffness with bending was largely due to the applied load being placed entirely on the AF, rather than being distributed between the AF and softer NP [7]. When bending was applied after compression, peak compressive stress was located near the NP-AF interface (Fig. 5(*a*)). The lack of the NP resulted in shift in peak compressive stress to the outer AF, a 50% increase in compressive stress, and a 25% increase in compressive strain. The 2:1 relative change in stress and strain with nucleotomy is likely due to the nonlinear mechanical properties of the AF, resulting in an increase in joint stiffness with bending [26,48] and may result in microtears to form or propagate within the AF [49], which has been observed with age and degeneration [45]. Moreover, the shift in compressive stress location during compression may contribute to disc joint instability [50].

Generally, dual loading with Nucleotomy resulted in an increase in bending stiffness, but joint stiffness decreased under axial rotation. Previous studies have shown that AF damage, as observed in herniated discs, results in a decrease in axial rotation stiffness [51–53]. The loss in torsional stiffness with annular injury was due to a reduction in fiber engagement, where only fibers in alternating layers experience loading [29]. This suggests that the Nucleotomy model likely underestimates the decrease in torsional stiffness, due to the posterior-lateral AF not being damaged in the model. Regardless, the findings from this study suggest that the decrease in torsional stiffness was largely due to differences in behavior that occurred during axial compression, where fibers reoriented toward the horizontal plane and the amount of fiber reorientation increased with nucleotomy. Our previous work showed that discs with fibers orientated closer to the horizontal plane have lower torsional stiffness and maximum shear strains [29]. More importantly, a decrease in torsional stiffness has been shown to occur in patients with lower back pain [54]. Taken together, this suggests that restoring torsional stiffness is an important target for biological repair strategies [55].

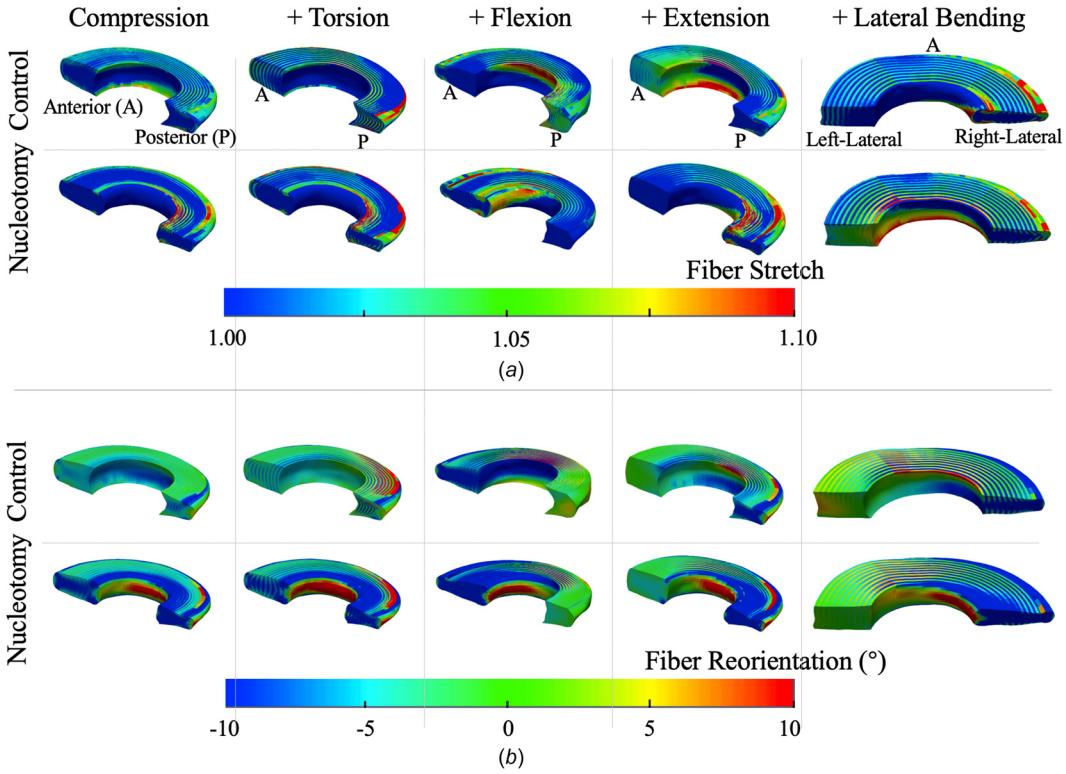

Fig. 8 (*a*) Fiber stretch and (*b*) reorientation for the Control (top row) and Nucleotomy (bottom row) model under torsion, flexion, extension, and lateral bending, which was applied after axial compression (represented by "+"). Positive values represent fiber reorientation toward the axial plane, whereas negative values represent reorientation toward the transverse plane. (Color version online.)

Large differences were observed in fiber stretch and engagement (Fig. 7). Fiber engagement under compression or torsion decreased with Nucleotomy. Therefore, fibers that were engaged during loading experienced greater strains (fiber stretch), which may make the inner AF more susceptible to damage accumulation. This agrees well with observations of herniated discs with more inner AF damage having a higher risk for reherniation [56]. Thus, NP repair strategies that repressurize the disc may act to decrease fiber stretch in the inner AF, reducing the risk of additional AF damage [57].

Surgical treatment for painful disc herniation requires a balance between relieving pain, reducing the risk of reherniation, and minimizing the amount of material removed. In this study, we evaluated an extreme case of nucleotomy; however, the actual amount of NP material removed during surgery can vary widely based on injury severity, disc health, and surgeons' approach. In healthy or moderately degenerated discs, the remaining NP may be able to swell further and partially maintain disc function, but the decrease in intradiscal pressure may cause degenerative changes, due to an increase in tensile radial strains [5].

The current model did not include facet joints or ligaments which may have altered the location and magnitude of peak stresses and strains for both the intact and nucleotomy models. Since much of the in vitro studies in the literature assess disc mechanics by removing spinal ligaments and facets, we chose to construct our model as a close representation of in vitro test specimens. Therefore, used in vitro experimental data for model validation and use the model to provide additional insights into disc mechanics that cannot be easily measured experimentally. The overall disc geometry was based on averaged information from 13 older (>50 years) and degenerated discs. However, material properties, lamellae structure, and NP area were based on data from healthy discs and model validation was conducted using data from discs that spanned a range of degeneration. While differences in data availability highlight challenges in developing and validating models for nondegenerate discs separate from degenerate discs, the findings regarding the effect of nucleotomy should apply to both healthy and degenerated discs.

Selection of incompressible or compressible material descriptions affects predicted stress magnitudes [58]. We described the NP and AF as having a compressible solid matrix [59], which may have predicted lower stresses and higher strains than a model that describes the solid matrix as being incompressible [20]. Load-controlled compression was applied to better represent in vivo loading (i.e., muscle forces and gravity); therefore, we assumed little to no change in muscle forces or body weight after nucleotomy. Angular rotations were restricted during axial compression, which resulted in reacting torques in both Control and Nucleotomy models. Thus, torque offset was subtracted to evaluate bending and torsional stiffness. The Nucleotomy model did not describe AF damage that typically occurs in the posterolateral region, which would affect the magnitude of stresses and strains near the injury site [60]. Finally, soft tissues in the model were described as hyperelastic materials, which does not account for time dependent behaviors. Thus, understanding the effect of nucleotomy on short-time scales (viscoelasticity) or long-time scales (tissue remodeling) could not be assessed, but is an important area of study.

In conclusion, the effect of nucleotomy on disc mechanics was dependent on the type and complexity of the applied loading condition. While disc joint stiffness decreased with nucleotomy under single loading conditions, as commonly reported in the literature, dual-loading conditions resulted in an increase in bending stiffness, agreeing with clinical observations. Dual loading with nucleotomy resulted in an increase in strain magnitude and altered the distribution of AF stresses and strains, which may lead to further damage accumulation and degenerative remodeling.

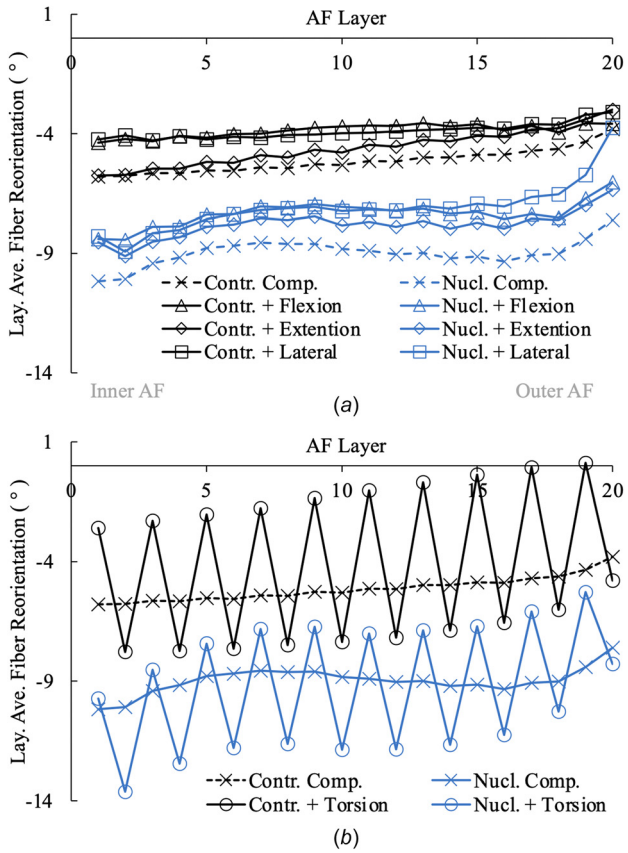

Fig. 9 Layer-averaged fiber reorientation for Control (black) and Nucleotomy (blue) models. (*a*) Flexion (triangles), extension (diamonds), lateral bending (squares), and (*b*) torsion (circles) was applied after axial compression. Positive values represent fiber reorientation toward the axial plane, while negative values represent reorientation toward the transverse plane. (Color version online.)

Authors' Contributions

Bo Yang and Grace D. O'Connell participated in study design, data analysis, data interpretation, and paper writing. Eric Klineberg participated in data interpretation and paper writing. Bo Yang performed all the simulations. All authors provided final approval for publication.

Funding Data

- Regents of the University of California (Funder ID: 10.13039/100005595).
- Signatures Innovation Fellowship from the University of California (Funder ID: 10.13039/100005595).
- National Science Foundation (NSF CAREER No. 1751212; Funder ID: 10.13039/100000001).

References

[1] O'Connell, G. D., Leach, J. K., and Klineberg, E. O., 2015, "Tissue Engineering a Biological Repair Strategy for Lumbar Disc Herniation," BioResearch Open Access, **4**(1), pp. 431–445.

[2] Cannella, M., Arthur, A., Allen, S., Keane, M., Joshi, A., Vresilovic, E., and Marcolongo, M., 2008, "The Role of the Nucleus Pulposus in Neutral Zone Human Lumbar Intervertebral Disc Mechanics," J. Biomech., **41**(10), pp. 2104–2111.

[3] Huang, J., Yan, H., Jian, F., Wang, X., and Li, H., 2015, "Numerical Analysis of the Influence of Nucleus Pulposus Removal on the Biomechanical Behavior of a Lumbar Motion Segment," Comput. Methods Biomech. Biomed. Eng., **18**(14), pp. 1516–1524.

[4] Meakin, J., and Hukins, D., 2000, "Effect of Removing the Nucleus Pulposus on the Deformation of the Annulus Fibrosus During Compression of the Intervertebral Disc," J. Biomech., **33**(5), pp. 575–580.

[5] O'Connell, G. D., Malhotra, N. R., Vresilovic, E. J., and Elliott, D. M., 2011, "The Effect of Discectomy and the Dependence on Degeneration of Human Intervertebral Disc Strain in Axial Compression," Spine, **36**(21), p. 1765.
[6] Seroussi, R. E., Krag, M. H., Muller, D. L., and Pope, M. H., 1989, "Internal Deformations of Intact and Denucleated Human Lumbar Discs Subjected to Compression, Flexion, and Extension Loads," J. Orthop. Res., **7**(1), pp. 122–131.
[7] Joshi, A. B., 2004, "Mechanical Behavior of the Human Lumbar Intervertebral Disc With Polymeric Hydrogel Nucleus Implant: An Experimental and Finite Element Study," Ph.D. dissertation, Drexel University, Philadelphia, PA.
[8] Meakin, J. R., Reid, J. E., and Hukins, D. W., 2001, "Replacing the Nucleus Pulposus of the Intervertebral Disc," Clin. Biomech., **16**(7), pp. 560–565.
[9] Strange, D. G. T., Fisher, S. T., Boughton, P. C., Kishen, T. J., and Diwan, A. D., 2010, "Restoration of Compressive Loading Properties of Lumbar Discs With a Nucleus Implant—A Finite Element Analysis Study," Spine J., **10**(7), pp. 602–609.
[10] Bezci, S. E., Eleswarapu, A., Klineberg, E. O., and O'Connell, G. D., 2018, "Contribution of Facet Joints, Axial Compression, and Composition to Human Lumbar Disc Torsion Mechanics," J. Orthop. Res., epub.
[11] Bezci, S. E., Klineberg, E. O., and O'Connell, G. D., 2018, "Effects of Axial Compression and Rotation Angle on Torsional Mechanical Properties of Bovine Caudal Discs," J. Mech. Behav. Biomed. Mater., **77**, pp. 353–359.
[12] O'Connell, G. D., Vresilovic, E. J., and Elliott, D. M., 2007, "Comparison of Animals Used in Disc Research to Human Lumbar Disc Geometry," Spine (Phila Pa 1976), **32**(3), pp. 328–333.
[13] Schmidt, H., Bashkuev, M., Dreischarf, M., Rohlmann, A., Duda, G., Wilke, H. J., and Shirazi-Adl, A., 2013, "Computational Biomechanics of a Lumbar Motion Segment in Pure and Combined Shear Loads," J. Biomech., **46**(14), pp. 2513–2521.
[14] Shirazi-Adl, A., Ahmed, A. M., and Shrivastava, S. C., 1986, "Mechanical Response of a Lumbar Motion Segment in Axial Torque Alone and Combined With Compression," Spine (Phila Pa 1976), **11**(9), pp. 914–927.
[15] Amin, D., Lawless, I., Sommerfeld, D., Stanley, R., Ding, B., and Costi, J., 2016, "The Effect of Six Degree of Freedom Loading Sequence on the In-Vitro Compressive Properties of Human Lumbar Spine Segments," J. Biomech., **49**(14), pp. 3407–3414.
[16] Berger-Roscher, N., Casaroli, G., Rasche, V., Villa, T., Galbusera, F., and Wilke, H.-J., 2017, "Influence of Complex Loading Conditions on Intervertebral Disc Failure," Spine, **42**(2), pp. E78–E85.
[17] Casaroli, G., Villa, T., Bassani, T., Berger-Roscher, N., Wilke, 1H.-J., and Galbusera, F., 2017, "Numerical Prediction of the Mechanical Failure of the Intervertebral Disc Under Complex Loading Conditions," Mater., **10**(1), p. 31.
[18] Ivicsics, M. F., Bishop, N. E., Puschel, K., Morlock, M. M., and Huber, G., 2014, "Increase in Facet Joint Loading After Nucleotomy in the Human Lumbar Spine," J. Biomech., **47**(7), pp. 1712–1717.
[19] Frei, H., Oxland, T. R., Rathonyi, G. C., and Nolte, L. P., 2001, "The Effect of Nucleotomy on Lumbar Spine Mechanics in Compression and Shear Loading," Spine (Phila Pa 1976), **26**(19), pp. 2080–2089.
[20] Shirazi-Adl, A., 1992, "Finite-Element Simulation of Changes in the Fluid Content of Human Lumbar Discs. Mechanical and Clinical Implications," Spine (Phila Pa 1976), **17**(2), pp. 206–212.
[21] Yang, B., Lu, Y., Um, C., and O'Connell, G. D., 2019, "Relative Nucleus Pulposus Area and Position Alters Disc Joint Mechanics," ASME J. Biomech. Eng., **141**(5), p. 051004.
[22] Peloquin, J. M., Yoder, J. H., Jacobs, N. T., Moon, S. M., Wright, A. C., Vresilovic, E. J., and Elliott, D. M., 2014, "Human L3L4 Intervertebral Disc Mean 3D Shape, Modes of Variation, and Their Relationship to Degeneration," J. Biomech., **47**(10), pp. 2452–2459.
[23] Moon, S. M., Yoder, J. H., Wright, A. C., Smith, L. J., Vresilovic, E. J., and Elliott, D. M., 2013, "Evaluation of Intervertebral Disc Cartilaginous Endplate Structure Using Magnetic Resonance Imaging," Eur. Spine J., **22**(8), pp. 1820–1828.
[24] Rodriguez, A. G., Rodriguez-Soto, A. E., Burghardt, A. J., Berven, S., Majumdar, S., and Lotz, J. C., 2012, "Morphology of the Human Vertebral Endplate," J. Orthop. Res., **30**(2), pp. 280–287.
[25] Marchand, F., and Ahmed, A. M., 1990, "Investigation of the Laminate Structure of Lumbar Disc Anulus Fibrosus," Spine, **15**(5), pp. 402–410.
[26] Holzapfel, G. A., Schulze-Bauer, C., Feigl, G., and Regitnig, P., 2005, "Single Lamellar Mechanics of the Human Lumbar Anulus Fibrosus," Biomech. Model. Mechanobiol., **3**(3), pp. 125–140.
[27] Skaggs, D. L., Weidenbaum, M., Iatridis, J. C., Ratcliffe, A., and Mow, V. C., 1994, "Regional Variation in Tensile Properties and Biochemical Composition of the Human Lumbar Anulus Fibrosus," Spine, **19**(12), pp. 1310–1319.
[28] Dreischarf, M., Zander, T., Shirazi-Adl, A., Puttlitz, C. M., Adam, C. J., Chen, C. S., Goel, V. K., Kiapour, A., Kim, Y. H., Labus, K. M., Little, J. P., Park, W. M., Wang, Y. H., Wilke, H. J., Rohlmann, A., and Schmidt, H., 2014, "Comparison of Eight Published Static Finite Element Models of the Intact Lumbar Spine: Predictive Power of Models Improves When Combined Together," J. Biomech., **47**(8), pp. 1757–1766.
[29] Yang, B., and O'Connell, G. D., 2017, "Effect of Collagen Fibre Orientation on Intervertebral Disc Torsion Mechanics," Biomech. Model. Mechanobiol., **16**(6), pp. 2005–2015.
[30] Cassidy, J., Hiltner, A., and Baer, E., 1989, "Hierarchical Structure of the Intervertebral Disc," Connect. Tissue Res., **23**(1), pp. 75–88.
[31] Beckstein, J. C., Sen, S., Schaer, T. P., Vresilovic, E. J., and Elliott, D. M., 2008, "Comparison of Animal Discs Used in Disc Research to Human Lumbar Disc: Axial Compression Mechanics and Glycosaminoglycan Content," Spine (Phila Pa 1976), **33**(6), pp. E166–E173.
[32] Heuer, F., Schmidt, H., Klezl, Z., Claes, L., and Wilke, H.-J., 2007, "Stepwise Reduction of Functional Spinal Structures Increase Range of Motion and Change Lordosis Angle," J. Biomech., **40**(2), pp. 271–280.
[33] Markolf, K. L., 1972, "Deformation of the Thoracolumbar Intervertebral Joints in Response to External Loads: A Biomechanical Study Using Autopsy Material," J. Bone Jt. Surg. Am., **54**(3), pp. 511–533.
[34] Cook, D. J., Yeager, M. S., Thampi, S. S., Whiting, D. M., and Cheng, B. C., 2015, "Range of Motion of the Intact Lumbar Segment: A Multivariate Study of 42 Lumbar Spines," Int. J. Spine Surg., **9**, p. 9.
[35] Pearcy, M., Portek, I., and Shepherd, J., 1984, "Three-Dimensional X-Ray Analysis of Normal Movement in the Lumbar Spine," Spine, **9**(3), pp. 294–297.
[36] Yamamoto, I., Panjabi, M. M., Crisco, T., and Oxland, T. O., 1989, "Three-Dimensional Movements of the Whole Lumbar Spine and Lumbosacral Joint," Spine (Phila Pa 1976), **14**(11), pp. 1256–1260.
[37] Maas, S. A., Ellis, B. J., Ateshian, G. A., and Weiss, J. A., 2012, "FEBio: Finite Elements for Biomechanics," ASME J. Biomech. Eng., **134**(1), p. 011005.
[38] Walter, B. A., Korecki, C. L., Purmessur, D., Roughley, P. J., Michalek, A. J., and Iatridis, J. C., 2011, "Complex Loading Affects Intervertebral Disc Mechanics and Biology," Osteoarthritis Cartilage, **19**(8), pp. 1011–1018.
[39] Reitmaier, S., Volkheimer, D., Berger-Roscher, N., Wilke, H.-J., and Ignatius, A., 2014, "Increase or Decrease in Stability After Nucleotomy? Conflicting In Vitro and In Vivo Results in the Sheep Model," J. R. Soc. Interface, **11**(100), p. 20140650.
[40] Costi, J. C. E. L., and O'Connell, G. D., 2020, "Spine Biomechanical Testing Methodologies: The Controversy of Consensus Vs Scientific Evidence," JOR Spine, Spec. Issue: Protoc., Methods, Resour. Spine Res., **4**(1), p. e1138.
[41] Zhou, M., Werbner, B., and O'Connell, G., 2020, "Historical Review of Combined Experimental and Computational Approaches for Investigating Annulus Fibrosus Mechanics," ASME J. Biomech. Eng., **142**(3), p. 030802.
[42] Yang, B., and O'Connell, G. D., 2019, "Intervertebral Disc Swelling Maintains Strain Homeostasis Throughout the Annulus Fibrosus: A Finite Element Analysis of Healthy and Degenerated Discs," Acta Biomater., **100**, pp. 61–74.
[43] Tavakoli, J., Amin, D. B., Freeman, B. J., and Costi, J. J., 2018, "The Biomechanics of the Inter- Lamellar Matrix and the Lamellae During Progression to Lumbar Disc Herniation: Which is the Weakest Structure?," Ann. Biomed. Eng., **46**(9), pp. 1280–12.
[44] Vernon-Roberts, B., Fazzalari, N. L., and Manthey, B. A., 1997, "Pathogenesis of Tears of the Annulus Investigated by Multiple-Level Transaxial Analysis of the T12-L1 Disc," Spine (Phila Pa 1976), **22**(22), pp. 2641–2646.
[45] Vernon-Roberts, B., Moore, R. J., and Fraser, R. D., 2007, "The Natural History of Age-Related Disc Degeneration: The Pathology and Sequelae of Tears," Spine (Phila Pa 1976), **33**(25), pp. 2767–2773.
[46] Putzier, M., Schneider, S. V., Funk, J. F., Tohtz, S. W., and Perka, C., 2005, "The Surgical Treatment of the Lumbar Disc Prolapse: Nucleotomy With Additional Transpedicular Dynamic Stabilization Versus Nucleotomy Alone," Spine, **30**(5), pp. E109–E114.
[47] Yorimitsu, E., Chiba, K., Toyama, Y., and Hirabayashi, K., 2001, "Long-Term Outcomes of Standard Discectomy for Lumbar Disc Herniation: A Follow-Up Study of More Than 10 Years," Spine (Phila Pa 1976), **26**(6), pp. 652–657.
[48] O'Connell, G. D., Guerin, H. L., and Elliott, D. M., 2009, "Theoretical and Uniaxial Experimental Evaluation of Human Annulus Fibrosus Degeneration," ASME J. Biomech. Eng., **131**(11), p. 111007.
[49] Werbner, B., Spack, K., and O'Connell, G. D., 2019, "Bovine Annulus Fibrosus Hydration Affects Rate-Dependent Failure Mechanics in Tension," J. Biomech., **89**, pp. 34–39.
[50] Wilke, H. J., Schmidt, H., Werner, K., Schmolz, W., and Drumm, J., 2006, "Biomechanical Evaluation of a New Total Posterior-Element Replacement System," Spine (Phila Pa 1976), **31**(24), pp. 2790–2796, discussion 2797.
[51] Elliott, D. M., Yerramalli, C. S., Beckstein, J. C., Boxberger, J. I., Johannessen, W., and Vresilovic, E. J., 2008, "The Effect of Relative Needle Diameter in Puncture and Sham Injection Animal Models of Degeneration," Spine (Phila Pa 1976), **33**(6), pp. 588–596.
[52] Michalek, A. J., Funabashi, K. L., and Iatridis, J. C., 2010, "Needle Puncture Injury of the Rat Intervertebral Disc Affects Torsional and Compressive Biomechanics Differently," Eur. Spine J., **19**(12), pp. 2110–2116.
[53] Michalek, A. J., and Iatridis, J. C., 2012, "Height and Torsional Stiffness Are Most Sensitive to Annular Injury in Large Animal Intervertebral Discs," Spine J., **12**(5), pp. 425–432.
[54] Haughton, V. M., Rogers, B., Meyerand, M. E., and Resnick, D. K., 2002, 1 "Measuring the Axial Rotation of Lumbar Vertebrae In Vivo With MR Imaging," AJNR Am. J. Neuroradiol., **23**(7), pp. 1110–1116.
[55] Long, R. G., Burki, A., Zysset, P., Eglin, D., Grijpma, D. W., Blanquer, S. B. G., Hecht, A. C., and Iatridis, J. C., 2016, "Mechanical Restoration and Failure Analyses of a Hydrogel and Scaffold Composite Strategy for Annulus Fibrosus Repair," Acta Biomater., **30**, pp. 116–125.
[56] Guterl, C. C., See, E. Y., Blanquer, S. B. G., Pandit, A., Ferguson, S. J., Benneker, L. M., Grijpma, D. W., Sakai, D., Eglin, D., Alini, M., Iatridis, J. C., and Grad, S., 2013, "Challenges and Strategies in the Repair of Ruptured Annulus Fibrosus," Eur. Cells Mater., **25**, pp. 1–21.
[57] Gorensek, M., Jaksimovic, C., Kregar-Velikonja, N., Gorensek, M., Knezevic, M., Jeras, M., Pavlovcic, V., and Cor, A., 2004, "Nucleus Pulposus Repair With Cultured Autologous Elastic Cartilage Derived Chondrocytes," Cell Mol. Biol. Lett., **9**(2), pp. 363–373.
[58] Nolan, D. R., Gower, A. L., Destrade, M., Ogden, R. W., and McGarry, J. P., 2014, "A Robust Anisotropic Hyperelastic Formulation for the

Modelling of Soft Tissue," J. Mech. Behav. Biomed. Mater., **39**, pp. 48–60.
[59] Ateshian, G. A., 2007, "On the Theory of Reactive Mixtures for Modeling Biological Growth," Biomech. Model. Mechanobiol., **6**(6), pp. 423–445.
[60] Vadalà, G., Russo, F., Pattappa, G., Schiuma, D., Peroglio, M., Benneker, L. M., Grad, S., Alini, M., and Denaro, V., 2013, "The Transpedicular Approach as an Alternative Route for Intervertebral Disc Regeneration," Spine, **38**(6), pp. E319–E324.